Theoretical study of the nonlinear optical properties of potassium titanyl phosphate (KTiOPO4): an extended Hueckel/sum-over-states approach

ARTICLE *in* CHEMISTRY OF MATERIALS · NOVEMBER 1992

Impact Factor: 8.35 · DOI: 10.1021/cm00024a033

3 AUTHORS, INCLUDING:

Richard Jarman
College of duPage
58 PUBLICATIONS **670** CITATIONS
SEE PROFILE

James F Harrison
Michigan State University
136 PUBLICATIONS **2,110** CITATIONS
SEE PROFILE

Theoretical Study of the Nonlinear Optical Properties of $KTiOPO_4$: An Extended Hückel/Sum-over-States Approach

M. Munowitz* and R. H. Jarman

Amoco Technology Company, P.O. Box 3011, Naperville, Illinois 60566-7011

J. F. Harrison

Department of Chemistry and Center for Fundamental Materials Research, Michigan State University, East Lansing, Michigan 48824-1322

Received June 5, 1992. Revised Manuscript Received August 12, 1992

We investigate, within the framework of extended Hückel theory, the origins and structural dependences of the electronic hyperpolarizability tensors of asymmetric TiO_2 and TiO_6^{8-}. The TiO_6^{8-} species, which is a basic structural unit of $KTiOPO_4$ (KTP), is taken as a distorted octahedron with the trans oxygens placed asymmetrically above and below the TiO_4 equatorial plane. A term-by-term analysis of the perturbative series for both TiO_2 and TiO_6^{8-} shows that second harmonic generation derives predominantly from π excitations (relative to the asymmetric O–Ti–O axis) and that the net hyperpolarizability results from the near cancellation of large contributions with opposite signs. Specific contributions to the hyperpolarizability, which we classify into three major π families and three major σ families, typically pass through minima and maxima as the difference between long and short Ti–O bonds is increased.

Introduction

With nonlinear optical phenomena such as second harmonic generation, optical parametric oscillation, and frequency mixing so important in the design of lasers and electrooptic devices, there remains sustained interest in developing and understanding new materials with suitable properties.[1,2] One well-known nonlinear system, potassium titanyl phosphate ($KTiOPO_4$, or KTP), has been used successfully for over 15 years to double the output of Nd:YAG lasers[3-7] and today serves as a model for a family of isomorphs and related inorganic structures.[8-15] A systematic microscopic analysis of the electronic hyperpolarizability of KTP therefore seems to be particularly desirable at this time, especially since any insight so gained may have implications for a broad class of systems important for both technological and theoretical reasons.

At the heart of KTP's crystal structure, and thought to be most relevant to its nonlinear optical properties, is a distorted TiO_6 octahedron in which the oxygens trans to the metal are positioned asymmetrically above and below an (approximately) planar TiO_4 grouping.[16] These octahedra are then linked, through shared corners, with distorted PO_4 tetrahedra to form a three-dimensional framework. The orthorhombic structure that results contains chains of –Ti–O–Ti–O– atoms running parallel to the crystallographic a axis, there being one oxygen shared between every two adjacent TiO_6 octahedra. The potassium atoms occupy sites in open hexagonal channels, as indicated in the projection shown in Figure 1.

KTP's large hyperpolarizability is generally attributed to the asymmetric disposition of the trans oxygens in the distorted TiO_6 octahedra, an arrangement which creates one unusually short (1.70–1.75 Å) and one unusually long (2.10–2.15 Å) Ti–O bond in each unit. Early studies using bond-parameter models for the nonlinear properties identified this structural and electronic feature as a key contributor to the microscopic hyperpolarizability.[3] More recent analyses using such models have pointed to the short bond, in particular, as largely determining the linear and nonlinear susceptibility.[17,18] Reported calculations of band structure made under the local density approximation, taking into account the potassium and phosphorus as well as the titanium and oxygen atoms, have also emphasized the dominant effect of the short Ti–O bonds on the electronic structure.[19] The more extended solid-state results suggest further that the TiO_6 and PO_4 groupings might act as localized electronic entities in the crystal and thus reinforce parallel studies made within the context of traditional molecular orbital theory.[13,14,20-22] These latter

(1) Chemla, D. S., Zyss, J., Eds. *Nonlinear Optical Properties of Organic Molecules and Crystals* (2 vols); Academic Press: Orlando, FL, 1987.
(2) Chen, C.-T.; Liu, G.-Z. *Annu. Rev. Mater. Sci.* **1986**, *16*, 203.
(3) Zumsteg, F. C.; Bierlein, J. D.; Gier, T. E. *J. Appl. Phys.* **1976**, *47*, 4980.
(4) Eimerl, D. *Proc. SPIE-Int. Soc. Opt. Eng.* **1986**, *681*, 5.
(5) Fan, T. Y.; Huang, C. E.; Hu, B. Q.; Eckhardt, R. C.; Fan, Y. X.; Byer, R. L.; Feigelson, R. S. *Appl. Opt.* **1987**, *26*, 2391.
(6) Vanherzeele, H.; Bierlein, J. D.; Zumsteg, F. C. *Appl. Opt.* **1988**, *27*, 3314.
(7) (a) Baumert, J. C.; Schellenberg, F. M.; Lenth, W.; Risk, W. P.; Bjorklund, G. C. *Appl. Phys. Lett.* **1987**, *51*, 2192. (b) Risk, W. P.; Baumert, J. C.; Bjorklund, G. C.; Schellenberg, F. M.; Lenth, W. *Appl. Phys. Lett.* **1988**, *52*, 85.
(8) Masse, R.; Grenier, J.-C. *Bull. Soc. Fr. Mineral. Cristallogr.* **1971**, *94*, 437.
(9) Marnier, G.; Boulanger, B.; Menaert. *J. Phys.: Condens. Matter* **1989**, *1*, 5509.
(10) El Haidouri, A.; Durand, J.; Cot, L. *Mater. Res. Bull.* **1990**, *25*, 1193.
(11) Crennell, S. J.; Owen, J. J.; Grey, C. P.; Cheetham, A. K.; Kaduk, J. A.; Jarman, R. H. *J. Mater. Chem.* **1991**, *1*, 113.
(12) Crennell, S. J.; Morris, R. E.; Cheetham, A. K.; Jarman, R. H. *Chem. Mater.* **1992**, *4*, 82.
(13) Stucky, G. D.; Phillips, M. L. F.; Gier, T. E. *Chem. Mater.* **1989**, *1*, 492.
(14) Phillips, M. L. F.; Harrison, W. T. A.; Gier, T. E.; Stucky, G. D.; Kulkarni, G. V.; Burdett, J. K. *Inorg. Chem.* **1990**, *29*, 2158.
(15) Phillips, M. L. F.; Harrison, W. T. A.; Stucky, G. D.; McCarron, E. M.; Calabrese, J. C.; Gier, T. E. *Chem. Mater.* **1992**, *4*, 222.
(16) Tordjman, I.; Masse, R.; Guitel, J. C. *Z. Kristallogr.* **1974**, *139*, 103.
(17) Hansen, N. K.; Protas, J.; Marnier, G. *C. R. Acad. Sci. Paris, Ser. II* **1988**, *307*, 475.
(18) Sastry, P. U. M. *Solid State Commun.* **1991**, *78*, 593.
(19) Ching, W. Y.; Xu, Y.-N. *Phys. Rev. B* **1991**, *44*, 5332.
(20) Chen, C. T.; Chen, X. S. *Commun. Fujian Inst. Struct. Matter* **1979**, *2*, 51.
(21) Jarman, R. H.; Munowitz, M.; Harrison, J. F. *J. Cryst. Growth* **1991**, *109*, 353.

0897-4756/92/2804-1296$03.00/0

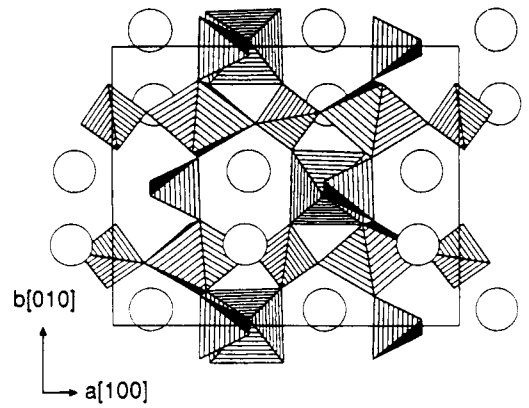

Figure 1. Crystal structure of $KTiOPO_4$, shown as a projection on the (001) plane. The drawing highlights the interconnected TiO_6 octahedra and PO_4 tetrahedra. The K atoms appear as large circles.

approaches have yielded descriptions of electronic structure and bonding at both the semiempirical and ab initio levels and provide the immediate background for the present work.

Our intention here is to explore the effects of geometric and electronic distortion on the hyperpolarizability tensors of TiO_2 and TiO_6^{8-} species, using these fragments as quasi-localized models for the crystalline KTP system. An extended Hückel treatment of the electronic wave function (which in subsequent work we plan to replace by self-consistent semiempirical and ab initio forms) provides a convenient, if qualitative, starting point for a perturbative evaluation of the nonlinear optical coefficients. The one-electron extended Hückel model has been used before in studies of KTP and related systems,[13,14,23,24] and indeed many of its qualitative aspects and predictions figure implicitly in conventional notions of chemical bonding.[25,26] The Hückel picture, its oversimplified assumptions notwithstanding, has the clear advantage of preserving both the full overlaps and the basic symmetries of the molecular orbitals while capturing many important features of electronic structure in a fashion that appeals to chemical intuition. In this way we are able to examine, rapidly and efficiently, a large number of structures and thus help to elucidate some of the factors that influence the nonlinear optical properties of KTP. The specific numerical results cannot be interpreted quantitatively, of course, nor can they be reasonably expected to reproduce experimental data in any absolute sense. Rather, our more modest goals are simply to understand the relative importance of various effects and to expose certain trends and tendencies within a carefully controlled series of model structures. What we do, specifically, is analyze the perturbative series for the hyperpolarizability tensor term by term while varying a single structural parameter. *Relative* effects within each well-defined family therefore should become apparent despite the inevitable inaccuracy of any individual result. Of particular interest are such questions as the effect of fragment size (scaling up from TiO_2 to TiO_6 and beyond), the distinct roles played by the π- and σ-electron systems, and how different classes of electronic excitations contribute to the hyperpolarizability. From the viewpoint of the materials chemist, such an analysis may offer some aid in eventually understanding structure–property relationships in KTP; from the more restricted viewpoint of the theoretical chemist, this systematic application of the extended Hückel model to second harmonic generation in inorganic materials may provide a useful basis for comparing one-electron and self-consistent approaches to the analysis of nonlinear optical effects.

It should be clear that our immediate intention is not to account for the bulk nonlinear susceptibility of the crystalline system. A complete understanding of KTP and related materials will certainly involve factors beyond the local electronic structure of the fragments we consider. Additional structural irregularities, the influence of the cation, local field effects, and, most notably, the extended chains and periodicity of the system all play a role in determining the nonlinear optical properties. Our goal at present is to contribute to this understanding by focusing on the smallest subunits of the crystal that can be expected to retain its essential properties. We suggest that this work might constitute a good beginning to the understanding of a very complex problem.

Formalism and Notation

Adopting the usual summation convention for repeated indexes, we define microscopic polarizability tensors of various ranks through the expression

$$p_i = \alpha_{ij}(\omega)E_j(\omega) + \beta_{ijk}(-\omega;\omega_1,\omega_2)\,E_j(\omega_1)\,E_k(\omega_2) + \gamma_{ijkl}(-\omega;\omega_1',\omega_2',\omega_3')\,E_j(\omega_1')\,E_k(\omega_2')\,E_l(\omega_3') + \ldots \quad (1)$$

where p_i $(i = x, y, z)$ is a component of the dipole moment induced in the molecule by time-dependent electric fields $\mathbf{E}(\omega)$. Second-order nonlinear effects are governed by the first hyperpolarizability tensor, β, which in the case of second harmonic generation (SHG) converts a single incident field oscillating at ω into an induced dipole moment oscillating at 2ω.

For position operators $\hat{R}_i(=x,y,z)$ acting on the electronic ground state $|g\rangle$ and excited states $|n\rangle$ and $|m\rangle$, we define the quantity $\langle ijk\rangle$ and its permutations as

$$\langle ijk\rangle = \langle g|\hat{R}_i|n\rangle\langle n|\hat{R}_j|m\rangle\langle m|\hat{R}_k|g\rangle \quad (2)$$

where the complete N-electron dipole moment operator

$$\hat{R}_i = \sum_{\alpha=1}^{N} r_{i\alpha} \quad (3)$$

is given as the sum of N individual electronic operators $r_{i\alpha}$.

Taking ω_n as the energy difference (in units of angular frequency) between $|n\rangle$ and $|g\rangle$, we then define expressions

$$f(2\omega,\omega) = [(\omega_n + 2\omega)(\omega_m + \omega)]^{-1} \quad (4a)$$

$$f(-2\omega,-\omega) = [(\omega_n - 2\omega)(\omega_m - \omega)]^{-1} \quad (4b)$$

$$f(\omega,-\omega) = [(\omega_n + \omega)(\omega_m - \omega)]^{-1} \quad (4c)$$

for each pair of excited states $|n\rangle$, $|m\rangle$. With this notation, the components of the SHG tensor are given by standard perturbation theory[27-29] as

$$\beta_{ijk}(-2\omega;\omega,\omega) = -(e^3/8\hbar^2)\sum_{n,m} 2\{(\langle ijk\rangle + \langle ikj\rangle) \times [f(2\omega,\omega) + f(-2\omega,-\omega)] + (\langle kij\rangle + \langle jik\rangle)f(\omega,-\omega)\} \quad (5)$$

Evaluation of β under the "sum-over-states" perturbative

(22) Munowitz, M.; Jarman, R. H.; Harrison, J. F. *J. Phys. Chem.* **1992**, *96*, 124.
(23) Burdett, J. K.; Hughbanks, T. *Inorg. Chem.* **1985**, *24*, 1741.
(24) Burdett, J. K. *Inorg. Chem.* **1985**, *24*, 2244.
(25) Hoffmann, R. *J. Chem. Phys.* **1963**, *39*, 1397.
(26) Janiak, C.; Hoffmann, R. *J. Am. Chem. Soc.* **1990**, *112*, 5924.
(27) Ward, J. F. *Rev. Mod. Phys.* **1965**, *37*, 1.
(28) Orr, J. B.; Ward, J. F. *Mol. Phys.* **1971**, *20*, 513.
(29) Pugh, D.; Morley, J. O. In *Nonlinear Optical Properties of Organic Molecules and Crystals*; Chemla, D. S., Zyss, J., Eds.; Academic Press: Orlando, FL, 1987; Vol. 1, pp 193–225.

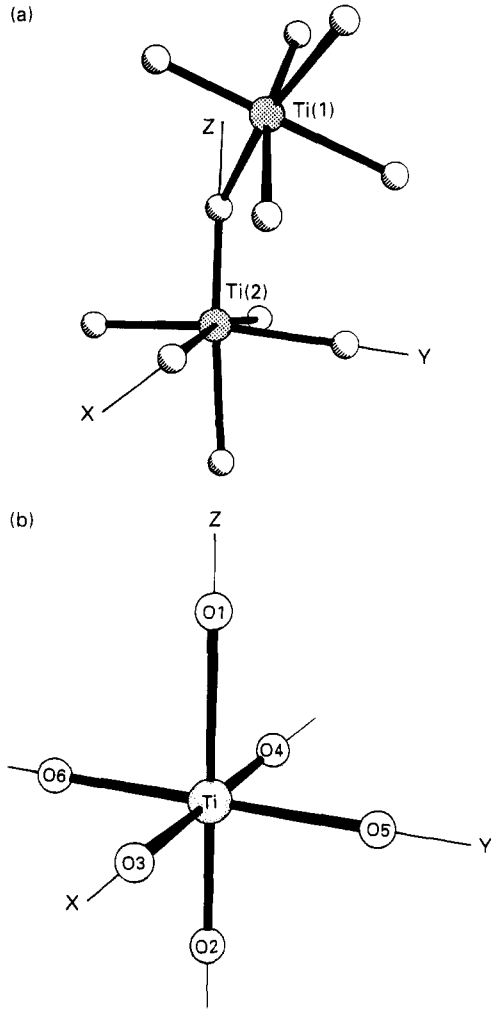

Figure 2. (a) The coordination spheres around the two titanium atoms in the KTP unit cell. (b) Idealized representation of the environment surrounding Ti(2). The axial O1–Ti–O2 group defines the z direction, and the planar TiO_4 group establishes the equatorial (xy) plane of the distorted octahedron.

approach thus amounts to computing the matrix elements in eq 2 and supplying the energies in eq 4.

The ground state is most conveniently written as a single closed-shell Slater determinant, while the excited states

$$|n\rangle = \sum_{a,\mu} A_{n,a\to u}|X_{a\to u}\rangle \tag{6}$$

obtained in general by configuration interaction, are linear combinations of singly-excited determinants $|X_{a\to u}\rangle$. Each configuration $|X_{a\to u}\rangle$ is an antisymmetrized product of one-electron molecular orbitals |a)|b)...|u)|v)... and differs from the ground state by the promotion of one electron from an occupied orbital |a) to a virtual orbital |u). (Note that we will consistently use the symbol $|...\rangle$ to denote determinantal states and |...) to refer to atomic or molecular orbitals.)

If the atomic coordinates are transformed into a reference frame where the ground-state electronic dipole moment, $-e\langle g|\hat{\mathbf{R}}|g\rangle$, is zero, then the transition moments are given by

$$\langle n|\hat{R}_i|m\rangle = \sum_{a\to u}\sum_{b\to v} A_{n,a\to u}A_{m,b\to v}[(u|r_i|v)\delta_{ab} - (a|r_i|b)\delta_{uv}] \tag{7a}$$

$$\langle g|\hat{R}_i|n\rangle = \sqrt{2}\sum_{a\to u} A_{n,a\to u}(a|r_i|u) \tag{7b}$$

according to the Slater–Condon rules.[30] The factor $\sqrt{2}$ appears in eq 7b because the ground state is a closed-shell singlet.

These expressions are simplified further in the Hückel picture, where in the absence of any interelectronic repulsion each excited state is obtained merely by shifting one electron from an occupied to a virtual orbital. Hence all but one coefficient is zero in eq 6, and the relevant matrix elements are then

$$\langle n|\hat{R}_i|m\rangle = (u|r_i|v)\delta_{ab} - (a|r_i|b)\delta_{uv} \tag{8a}$$

$$\langle g|\hat{R}_i|n\rangle = \sqrt{2}(a|r_i|u) \tag{8b}$$

The molecular orbitals themselves are taken as linear combinations of atomic orbitals $|\mu)$:

$$|a) = \sum_{\mu} c_{\mu a}|\mu) \tag{9}$$

with each atomic basis function

$$|\mu) = \sum_{k} d_{k\mu}\phi_k \tag{10}$$

expressed as a contracted sum of Gaussian primitives ϕ_k in order to facilitate computation of the overlap integrals, S_{ij}, required in the extended Hückel calculation. The Gaussians are understood to be in standard form (not explicitly normalized):

$$\phi_k(\xi,r) = w_k(x,y,z)\exp(-\xi r^2) \tag{11}$$

where the angular function $w(x,y,z)$ takes the value 1 for s orbitals; x, y, and z for p orbitals, and x^2-y^2, $3r^2-z^2$, xy, xz, and yz for d orbitals. Orbital exponents ξ, contraction coefficients $d_{k\mu}$, and Hückel parameters H_{ii} are provided in Table I. Interaction integrals H_{ij} are estimated as $-1.75S_{ij}(H_{ii}H_{jj})^{1/2}$ under the modified Wolfsberg–Helmholtz approximation.

Model Systems

Geometric Structure. Figure 2a shows the actual arrangement of atoms belonging to two adjacent TiO_6 octahedra in the KTP crystal structure. Each titanium occupies a distinct crystallographic site, with four of its surrounding oxygens coordinated to phosphorus atoms while the other two are linked to neighboring titanium atoms.

We take as a model for the Ti(2) site a single distorted TiO_6^{8-} octahedron, idealized as having, at most, C_{4v} symmetry and envisioned as arising from Ti^{4+} and O^{2-} species:

$$Ti^{4+} + 6O^{2-} \rightarrow TiO_6^{8-}$$

A TiO_2 fragment, similarly arising as

$$Ti^{4+} + 2O^{2-} \rightarrow TiO_2$$

is considered as well in order to further isolate the effects of the long and short Ti–O bonds.

The TiO_6^{8-} model has been used previously in consideration of nonlinear optical effects in KTP, and we adopt it here partly to simplify comparison with such work.[13,14] Both this particular species and the simpler TiO_2 have the advantages, moreover, of being derived entirely from closed-shell constituents and of offering high symmetry.

We label as O1 and O2, respectively, the oxygens in the long and short Ti–O bonds of TiO_6^{8-}, taking these trans to the metal along the z axis. Each of the remaining four oxygens (labeled O3, O4, O5, and O6) is placed along one of the directions in the xy plane, and the titanium is positioned at the origin. The relevant coordinate system

(30) Szabo, A.; Ostlund, N. S. *Modern Quantum Chemistry: Introduction to Advanced Electronic Structure Theory*; Macmillan: New York, 1982.

Table I. Orbital Parameters

orbital	H_{ii} (eV)	exponent	coefficient
Ti 4s	−9.79	0.262 088 68	−0.087 431 45
		0.051 404 26	0.081 307 29
		0.025 369 38	0.005 693 26
Ti 4p	−6.027	0.221 419 73	−0.013 310 12
		0.033 853 93	0.013 670 04
		0.016 645 53	0.003 351 56
Ti 3d	−12.11	10.825 600 00	6.552 054 74
		3.394 380 00	2.984 788 09
		1.322 190 00	0.397 669 41
		1.024 910 00	0.197 323 37
		0.321 362 00	0.089 890 83
		0.125 177 00	0.011 976 16
O 2s	−32.3	13.361 281 71	−0.298 570 80
		0.811 342 41	0.363 151 27
		0.311 486 30	0.136 152 03
O 2p	−14.8	4.757 630 66	1.626 487 63
		1.221 030 60	1.035 847 46
		0.414 557 52	0.200 239 41

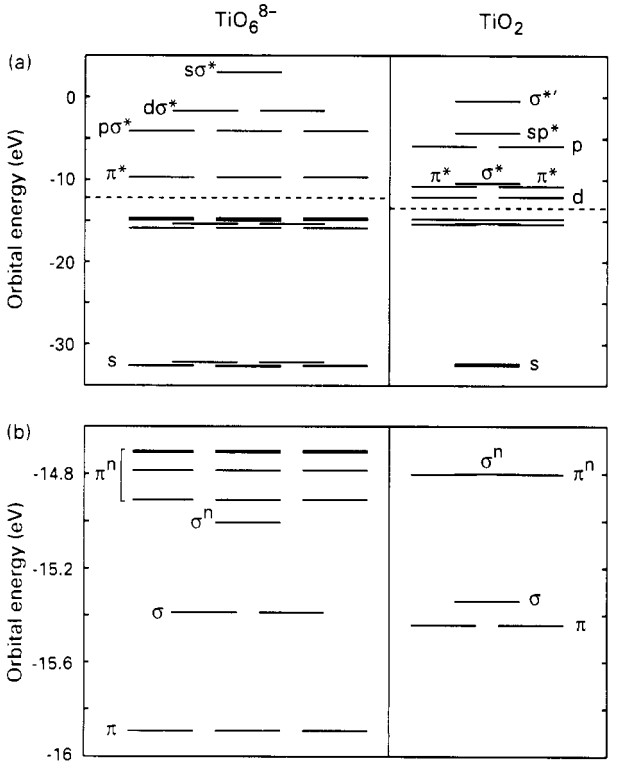

Figure 3. Energy levels for TiO_6^{8-} and TiO_2, from extended Hückel calculations using the parameters in Table I. Equal bond lengths of 1.96 Å are used throughout. (a) Full set. (b) Expanded view showing the highest occupied levels, which are unlabeled in the diagram above. Many of the states are nearly degenerate. Also, some of the π^n orbitals exhibit σ^n character along one or more axes. For clarity, we omit a detailed description of these. It is also noted that upon distortion of the octahedron and removal of the triple degeneracy, the combination of the p orbitals in the different levels varies slightly.

is shown in Figure 2b. In considering deviations from octahedral symmetry we systematically vary, as in earlier studies,[13,14] the axial Ti–O1 and Ti–O2 bond distances around some average value r_0 by defining a quantity $\Delta = r(\text{Ti–O1}) - r(\text{Ti–O2})$:

$$r(\text{Ti–O1}) = r_0 + \Delta/2 \quad (12a)$$

$$r(\text{Ti–O2}) = r_0 - \Delta/2 \quad (12b)$$

The four equatorial (xy) Ti–O bonds in the TiO_6^{8-} species are fixed at r_0.

Energy levels for symmetric TiO_6^{8-} and TiO_2 (r_0 = 1.96 Å, Δ = 0) are summarized in Figure 3, with the full set

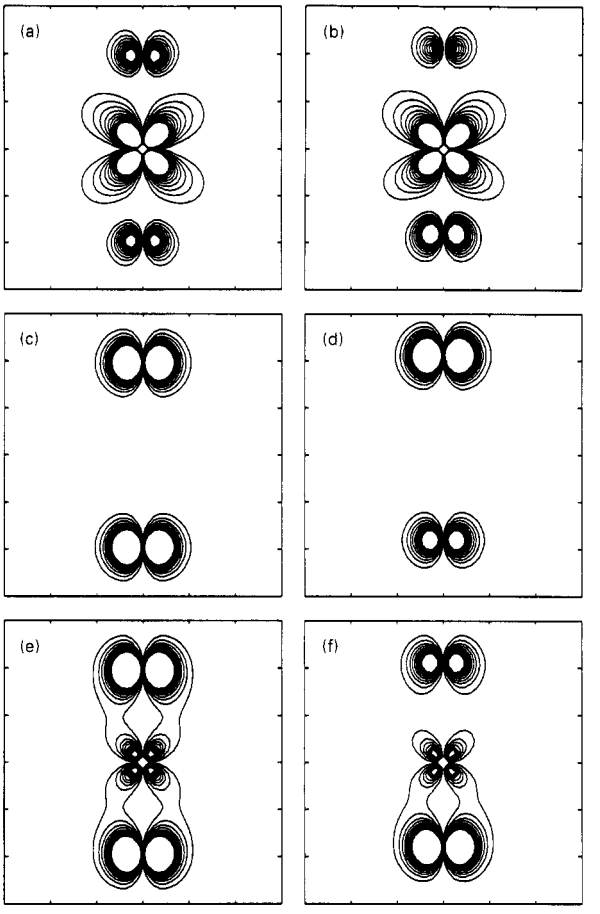

Figure 4. Electronic density for one set of π orbitals in TiO_2, viewed in the xz plane. Bonding and antibonding orbitals derive from the appropriate combination of $|\text{Ti}_{xz}\rangle$, $|\text{O1}_x\rangle$, and $|\text{O2}_x\rangle$, whereas the nonbonding combination involves only $|\text{O1}_x\rangle$ and $|\text{O2}_x\rangle$. The weighting of the oxygen atomic orbitals is equal when $\Delta = 0$. Equally spaced contours are shown for the lowermost 20% of the surface. (a) Antibonding, $\Delta = 0$. (b) Antibonding, Δ = 0.3 Å. (c) Nonbonding, $\Delta = 0$. (d) Nonbonding, Δ = 0.3 Å. (e) Bonding, $\Delta = 0$. (f) Bonding, Δ = 0.3 Å. Average bond length is 1.96 Å. The distant oxygen, O1, is positioned at the top of each 6 Å × 6 Å grid, and the titanium is at the center.

shown in the top panel and an expanded view of the uppermost occupied orbitals given below. In each panel, the diagram at the left pertains to TiO_6^{8-} while that on the right pertains to TiO_2. These levels and the corresponding molecular orbital combinations evolve smoothly with Δ as the structures are varied from the original symmetric arrangements.

In TiO_2 there are four classes of occupied orbitals (σ^n, π^n, σ, π) and two relevant classes of unoccupied orbitals (π^*, σ^*) falling within a relatively narrow band of energy, and it is this subset of the total that is expected to contribute most to the hyperpolarizability. Contours of electronic density for $|\pi\rangle$, $|\pi^n\rangle$, and $|\pi^*\rangle$ in TiO_2 groups with $\Delta = 0$ and Δ = 0.3 Å (r_0 = 1.96 Å) are presented in Figure 4 to give a sense for the shapes of the orbitals and the effect of the distortion in a structure close to that existing in the KTP crystal; an equivalent set of contour plots for the $|\sigma\rangle$, $|\sigma^n\rangle$, and $|\sigma^*\rangle$ functions is provided in Figure 5. Note that the σ^n and π^n combinations are taken as nonbonding with respect to titanium.

Many of the orbitals identified in TiO_2 are found in TiO_6^{8-} as well, appropriately modified to reflect the participation of the equatorial oxygens in the xy plane. The most important combinations in TiO_6^{8-} for $\Delta = 0$ and Δ = 0.3 Å (r_0 = 1.96 Å) are depicted in Figures 6 and 7 by contour plots showing electron density in the xz plane for

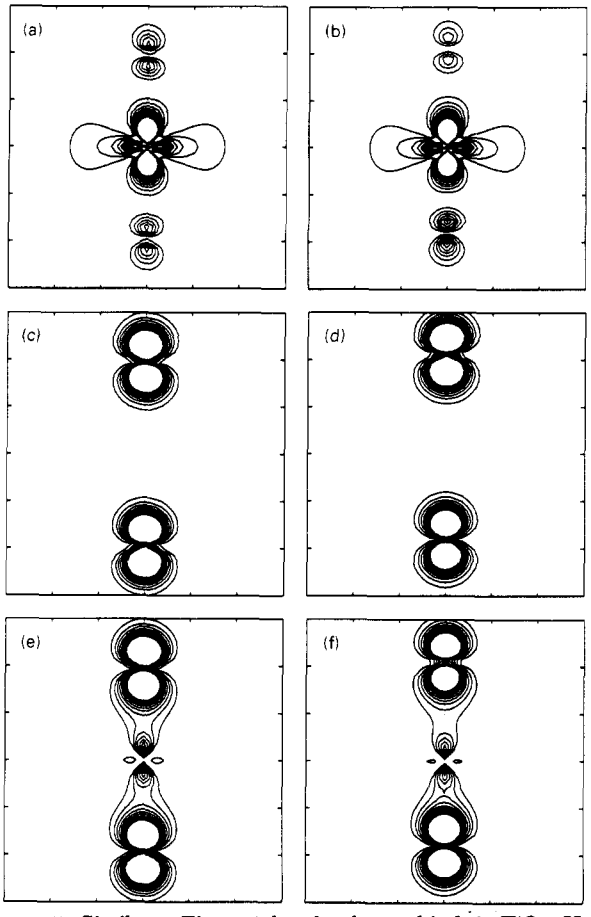

Figure 5. Similar to Figure 4, but for the σ orbitals in TiO_2. Here the bonding and antibonding combinations involve $|Ti_z\rangle$, $|O1_z\rangle$, and $|O2_z\rangle$, while the nonbonding form includes only $|O1_z\rangle$ and $|O2_z\rangle$.

representative π, π^n, π^*, σ, σ^n, and σ^* levels.

Second Harmonic Generation

The graphs in Figure 8 show values of β_{zzz}, β_{zxx} ($=\beta_{zyy}$), and β_{xxz} ($=\beta_{xzx} = \beta_{yyz} = \beta_{yzy}$) at 1064 nm, obtained by substituting expressions 2, 4, and 8 into eq 5. All plots are presented with the same vertical and horizontal axes for ease of comparison, and units of β are 10^{-30} cgs. Tensor indices refer to the coordinate system of Figure 2b.

All singly-excited states were used in the calculations, and points were computed for TiO_2 and TiO_6^{8-} with the parameters r_0 = 1.86, 1.96, and 2.06 Å and Δ = 0.0, 0.1, ..., 0.7 Å. An average Ti–O bond distance of 1.96 Å is typical for rutile structures; the combination of r_0 = 1.96 Å and Δ = 0.3–0.4 Å, in particular, gives long and short bonds reasonably close to those in KTP.

The component β_{zzz} has the largest magnitude in both TiO_2 and TiO_6^{8-}, an obvious consequence of the asymmetric O1–Ti–O2 group. All other nonzero components, which involve either input or output polarizations in the xy plane, are negligible for TiO_2.

Note that the β_{zzz} curves for TiO_2 exhibit extrema at intermediate values of Δ, whereas those for TiO_6^{8-} appear to level off at the largest distortions. The signs of β_{zzz} are consistently opposite for the two species as well. We now consider a term-by-term analysis of eq 5 in order to understand the detailed origins of these gross features and to assess their significance.

Each pair of excited states, $|n\rangle$ and $|m\rangle$, contributes to β as part of the quantity $\langle g|\hat{\mathbf{R}}|n\rangle\langle n|\hat{\mathbf{R}}|m\rangle\langle m|\hat{\mathbf{R}}|g\rangle$, which may be visualized as in Figure 9. Having already identified the principal features of the molecular orbitals, we

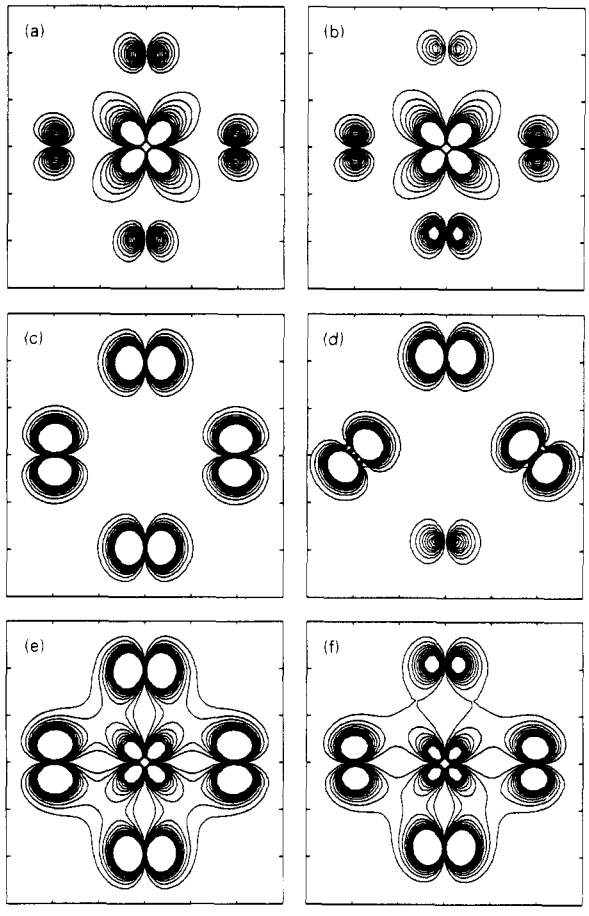

Figure 6. Density contours for the π orbitals in TiO_6^{8-}, as in Figure 4. The bonding and antibonding forms appear in groups of three, with each member being a mixture of an off-diagonal titanium d orbital, here $|Ti_{xz}\rangle$, and four coplanar oxygen p orbitals. The oxygens appear with equal weight when Δ = 0, and the resulting three t_{2g} levels are degenerate under full octahedral symmetry. The nonbonding orbital shown here is only one of many; for additional comment, see note 31.

can group the various products of dipole transition moments into a set of three excitations within the π system:

A: $$|n\rangle = |m\rangle = |\pi^n \rightarrow \pi^*\rangle$$

B: $$|n\rangle = |\pi^n \rightarrow |\pi^*\rangle, \quad |m\rangle = |\pi \rightarrow \pi^*\rangle$$

C: $$|n\rangle = |m\rangle = |\pi \rightarrow \pi^*\rangle$$

and a similar set of three within the σ system:

D: $$|n\rangle = |m\rangle = |\sigma^n \rightarrow \sigma^*\rangle$$

E: $$|n\rangle = |\sigma^n \rightarrow \sigma^*\rangle, \quad |m\rangle = |\sigma \rightarrow \sigma^*\rangle$$

F: $$|n\rangle = |m\rangle = |\sigma \rightarrow \sigma^*\rangle$$

These categories provide a convenient way to separate different contributions to β in the perturbative expression and, with the aid of relationship 8 for the matrix elements, enable us to concentrate on excitations involving only four types of occupied orbitals (π, π^n, σ, σ^n) and two types of unoccupied orbitals (π^*, σ^*).

π and σ Excitations in TiO_2. With a basis set of 17 atomic orbitals (one s, three p, and five d functions for titanium; one s and three p functions for each oxygen), there are 72 excited states for TiO_2 and thus 5184 possible pairs of $|n\rangle$ and $|m\rangle$. Of this total, however, only a select number contribute appreciably to β, since, when arranged in decreasing order, the absolute values of each term in eq 5 drop by more than 3 orders of magnitude over the first two dozen pairs of states. In Figure 10a, for r_0 = 1.96 Å

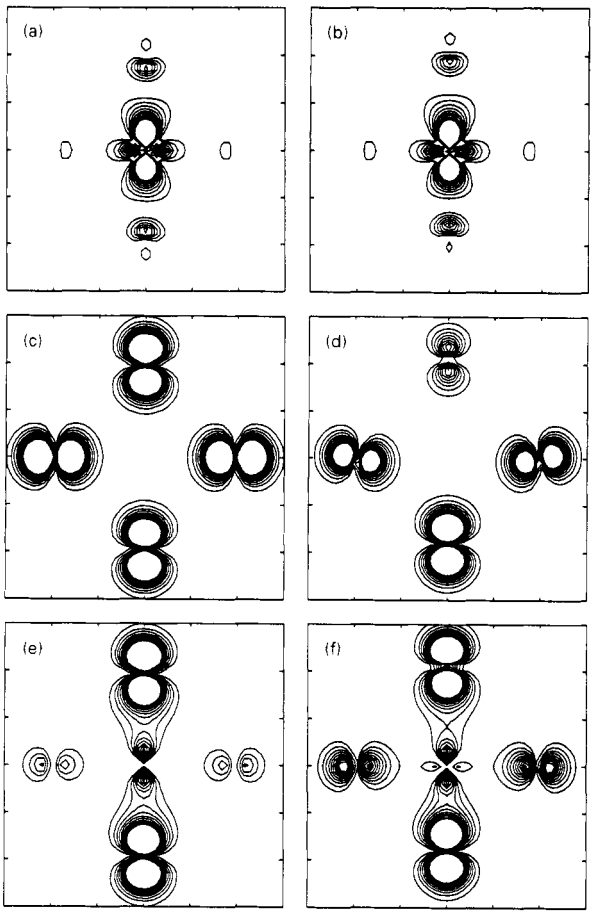

Figure 7. Similar to Figure 6, but for the σ orbitals in TiO_6^{8-}. Two σ bonding orbitals, which mix the components $|Ti_{x^2-y^2}\rangle$, $|Ti_{z^2}\rangle$, $|O1_z\rangle$, $|O2_z\rangle$, $|O3_x\rangle$, $|O4_x\rangle$, $|O5_y\rangle$, and $|O6_y\rangle$, become the doubly degenerate e_g levels when $\Delta = 0$. A corresponding pair of antibonding combinations exist, as do other antibonding arrangements involving titanium and oxygen p and s orbitals and, to varying extents, the titanium d_{z^2}. These σ functions are similar to the one in TiO_2, but the higher symmetry of TiO_6^{8-} allows additional mixing of the $d_{x^2-y^2}$ with the equatorial oxygen p orbitals. There is, finally, a single nonbonding σ combination involving all six oxygen orbitals along the coordinate axes.

we compare values of β_{zzz} obtained from complete sums over states with those obtained from partial sums over just these largest contributions. The partial sum consists entirely of excitations belonging to the six families A–F, and the good agreement between the two curves indicates that this subset of terms closely tracks the behavior of the full system.

Next, in Figure 10b we decompose the partial sum (A + B + C + D + E + F) into a π set (A + B + C) and a σ set (D + E + F) to see immediately that the nonlinear susceptibility is determined largely by π excitations. The extremum in the curve arises entirely from the π contribution, while the σ contribution grows steadily but modestly over the range of distortions considered.

Principal members of the A family include the degenerate $|\pi_x^n \rightarrow \pi_x^*\rangle$ and $|\pi_y^n \rightarrow \pi_y^*\rangle$ states; similarly, the C family is formed by the $|\pi_x \rightarrow \pi_x^*\rangle$ and $|\pi_y \rightarrow \pi_y^*\rangle$ states. The off-diagonal B terms include the four possible combinations of nonbonding $\rightarrow$ antibonding and bonding $\rightarrow$ antibonding transitions. The separate contributions made to β by A, B, and C are shown in Figure 11a, where we see that the A and B curves are both large but opposite in sign. Values on the C curve, reflecting the effect of diagonal bonding $\rightarrow$ antibonding excitations, are smallest at all values of Δ, although comparable in magnitude to the difference of A and B. It is through this small difference between two sets of larger numbers that the extremum in the curve is preserved in a reduced form.

A similar presentation for the σ system, with a different scale used for the vertical axis, is made in Figure 11b. Again the net contribution arises as a difference between two larger numbers of opposite sign, D and E, while here the F terms are virtually zero. Moreover, in overall appearance the D and E curves are similar to A and B and may in fact pass through extreme points near $\Delta = 0.6$ Å. We should stress, however, that such subtle differences in the shapes of the curves are probably far beyond the limitations of the present model.

Transition Dipole Moments in TiO_2. The relevant matrix elements for the π excitations may be reduced to integrals over molecular orbitals according to eq 8:

$$\text{I} \quad \langle g|\hat{Z}|\pi \rightarrow \pi^*\rangle = \sqrt{2}(\pi|z|\pi^*) \tag{13a}$$

$$\text{II} \quad \langle g|\hat{Z}|\pi^n \rightarrow \pi^*\rangle = \sqrt{2}(\pi^n|z|\pi^*) \tag{13b}$$

$$\text{III} \quad \langle \pi \rightarrow \pi^*|\hat{Z}|\pi^n \rightarrow \pi^*\rangle = -(\pi|z|\pi^n) \tag{13c}$$

$$\text{IV} \quad \langle \pi \rightarrow \pi^*|\hat{Z}|\pi \rightarrow \pi^*\rangle = (\pi^*|z|\pi^*) - (\pi|z|\pi) \tag{13d}$$

$$\text{V} \quad \langle \pi^n \rightarrow \pi^*|\hat{Z}|\pi^n \rightarrow \pi^*\rangle = (\pi^*|z|\pi^*) - (\pi^n|z|\pi^n) \tag{13e}$$

from which (using the notation I, II, ..., above) the products $\langle g|\hat{Z}|n\rangle\langle n|\hat{Z}|m\rangle\langle m|\hat{Z}|g\rangle$ follow as $II^2 \cdot V$, $I \cdot II \cdot III$, and $I^2 \cdot IV$ for A, B, and C, respectively.

Matrix elements IV and V therefore become equal to the difference in dipole moment between the π^* electron distribution and either the π or π^n, whereas the remaining integrals are proportional to transition moments involving given pairs of the $|\pi\rangle$, $|\pi^n\rangle$, and $|\pi^*\rangle$ molecular orbitals. Electron distributions corresponding to the three π orbitals have already been shown in Figure 4. At this point we plot the negatives of the molecular integrals separately in Figure 12 to demonstrate how the maxima and minima arise in the final products. The overall value for each family (in atomic units) is the result of two opposing trends, with one matrix element increasing as a function of Δ while the others decrease.

The algebraic signs and relative magnitudes of these integrals can be understood by using eq 13 and Figures 4–7. For example, the matrix element associated with family A is proportional to

$$|\langle g|\hat{Z}|\pi^n \rightarrow \pi^*\rangle|^2 \langle \pi^n \rightarrow \pi^*|\hat{Z}|\pi^n \rightarrow \pi^*\rangle$$

and the sign is carried by

$$\langle \pi^n \rightarrow \pi^*|\hat{Z}|\pi^n \rightarrow \pi^*\rangle = (\pi^*|z|\pi^*) - (\pi^n|z|\pi^n)$$

From Figure 4 we see that the molecular integrals $(\pi^*|z|\pi^*)$ and $(\pi^n|z|\pi^n)$ are both zero, by symmetry, when $\Delta = 0$. As the difference in bond lengths grows, electronic density in the π^n orbital shifts toward the distant oxygen (on the positive z axis), whereas in the π^* the shift is toward the near oxygen (along the negative z axis). As a result, $(\pi^n|z|\pi^n)$ increases more rapidly than $(\pi^*|z|\pi^*)$ and is positive. The overall sign of the family A matrix element is therefore negative, as is consistent with the explicit calculation in Figure 12a. (But note that the quantities plotted in Figure 12 are proportional to electronic dipole moments, $-e\langle z\rangle$, and that it is the product of three such matrix elements that produces the factor $-e^3$ in eq 5.)

In Figure 13 we show for families A, B, and C the values of the energy factors f as defined in eq 4. These curves increase steadily with Δ, changing by approximately 35% over the range shown, but run nearly parallel throughout. As a result, they play little role in introducing any differences among the three families contributing to β.

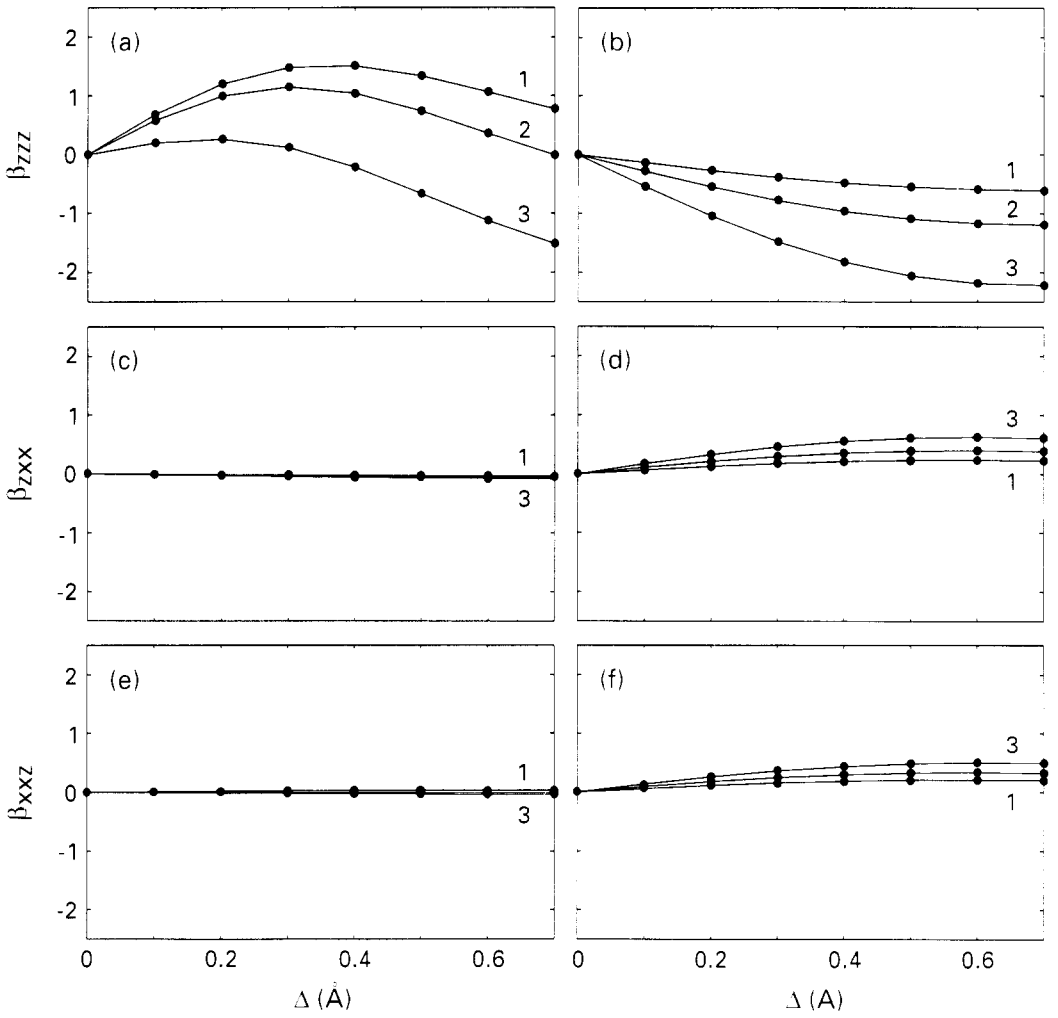

Figure 8. Nonzero components of β for TiO_2 and TiO_6^{8-} (at 1064 nm, in units of 10^{-30} cgs), shown as point-to-point plots versus Δ. Average Ti–O bond distances are 1.86 Å (curve 1), 1.96 Å (curve 2), and 2.06 Å (curve 3). (a) β_{zzz}, TiO_2. (b) β_{zzz}, TiO_6^{8-}. (c) β_{zxx}, TiO_2. (d) β_{zxx}, TiO_6^{8-}. (e) β_{xxz}, TiO_2. (f) β_{xxz}, TiO_6^{8-}. The same vertical scale applies to all the graphs.

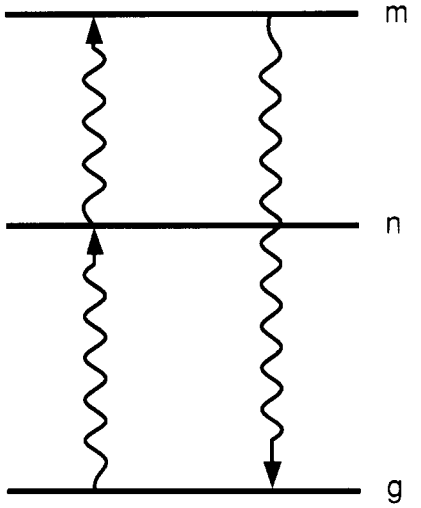

Figure 9. The matrix element $\langle g|\hat{R}|n\rangle\langle n|\hat{R}|m\rangle\langle m|\hat{R}|g\rangle$, pictured as three virtual transitions involving states $|g\rangle$, $|n\rangle$, and $|m\rangle$. Each transition may be polarized along any of the coordinate axes.

π and σ Excitations in TiO_6^{8-}. There are 216 singly-excited states in TiO_6^{8-} and thus 46 656 combinations that contribute to β_{zzz}. Of these we arbitrarily select the 100 terms with the largest absolute values and plot both the partial sum A + B + C + D + E + F and the complete sum in Figure 14a. As with TiO_2, the partial sum provides an excellent approximation despite certain minor irregularities. The jagged features apparent in the point-to-point plot arise from the arbitrary cutoff after 100 components. This set of values is closely spaced, and not every family is represented by the same number of contributions at each Δ; hence, there is some slight variation about the limiting values. Magnitudes decrease approximately 5-fold over the 20 largest terms, and drop by a factor 100–200 over the first 100.

There are more orbitals in TiO_6^{8-} than in TiO_2, but we adhere to the same basic description of families A–F as before. One necessary modification is the inclusion of all nonbonding π and σ orbitals where appropriate in A, B, D, and E. Various families also contain small components from new sources (for example, in B, a rare excitation from a combination of equatorial oxygen s orbitals to the π^* orbital), but these are generally insignificant. We include them for the sake of consistency and to preserve a reasonably compact description. In all cases, however, the 50 or so largest contributions are dominated by A and B terms.

Figure 14b, similar to Figure 10b, shows the breakdown of β_{zzz} into π and σ terms. Again the hyperpolarizability is mostly a consequence of the π electrons, even more so than in TiO_2. The assumption that π excitations alone should determine the nonlinear optical properties of KTP is consistent with certain elementary pictures of bonding, and has been made before albeit without the support of explicit calculations.[13,14] Nevertheless, the apparent exclusion of σ effects is not obvious given the favorable

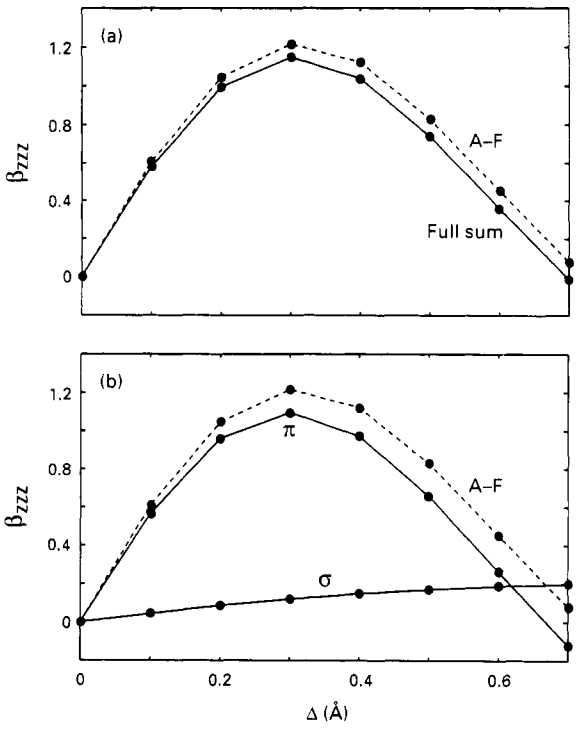

Figure 10. Point-to-point plots of β_{zzz} for TiO_2 (r_0 = 1.96 Å), decomposed into π and σ contributions. (a) Values calculated using all singly-excited states (solid curve), compared with partial sum A + B + C + D + E + F as described in the text (broken curve). (b) Partitioning into separate π (A + B + C) and σ (D + E + F) terms.

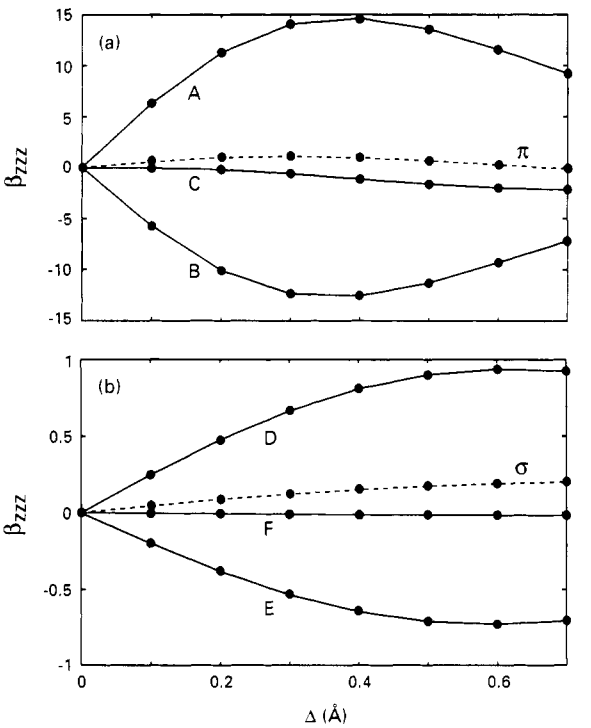

Figure 11. Further analysis of β_{zzz} in TiO_2. (a) Individual π terms (A, B, C), with the sum shown as the broken curve. (b) Similar, for the σ terms (D, E, and F). Note the different vertical scales.

position of the σ orbitals on the energy level diagram. In previous ab initio studies of a similar distorted octahedral structure, $Ti(OH)_4O_2^{2-}$, we have found that the dp σ orbital, which is filled in the ground state, can mediate a transfer of charge from the distant to the near oxygen.[22] Such a mechanism could lead to an enhanced excited-state dipole moment and thereby affect β, but this effect is not

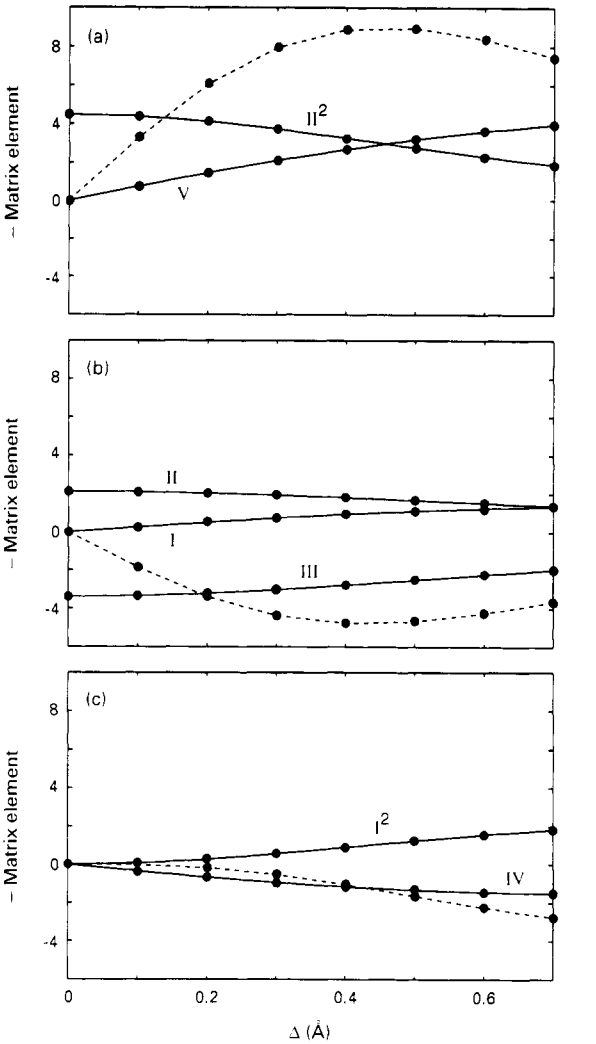

Figure 12. Dipole transition moments for each family of π excitations in TiO_2. Matrix elements (in atomic units; 1 bohr = 0.529 Å) are labeled as in eq 13, and the product of the three integrals is shown as the broken curve in each panel. (a) Family A. (b) Family B. (c) Family C. Note the change in sign relative to the previous figures.

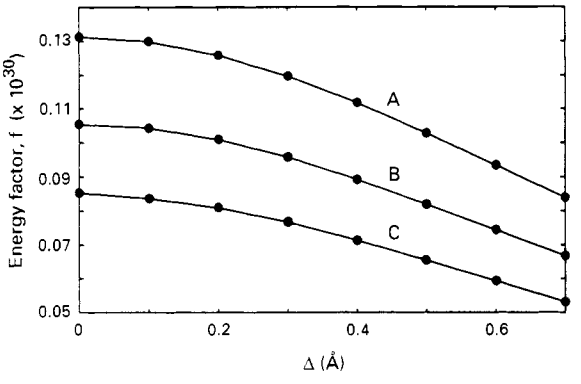

Figure 13. Sum of the corresponding energy factors, f, associated with β_{zzz} for the π excitations in TiO_2.

evident in the present model.

A final breakdown of the π terms into separate A, B, and C curves is provided in Figure 14c. It is apparent that, in this context, TiO_6^{8-} shares the same basic features with TiO_2—namely large values with opposite signs for A and B, maxima and minima in the A and B curves, and a steadily increasing, but still small, C curve. We note that the B term alone in TiO_6^{8-} has been examined previously using extended Hückel wave functions.[13,14] The present

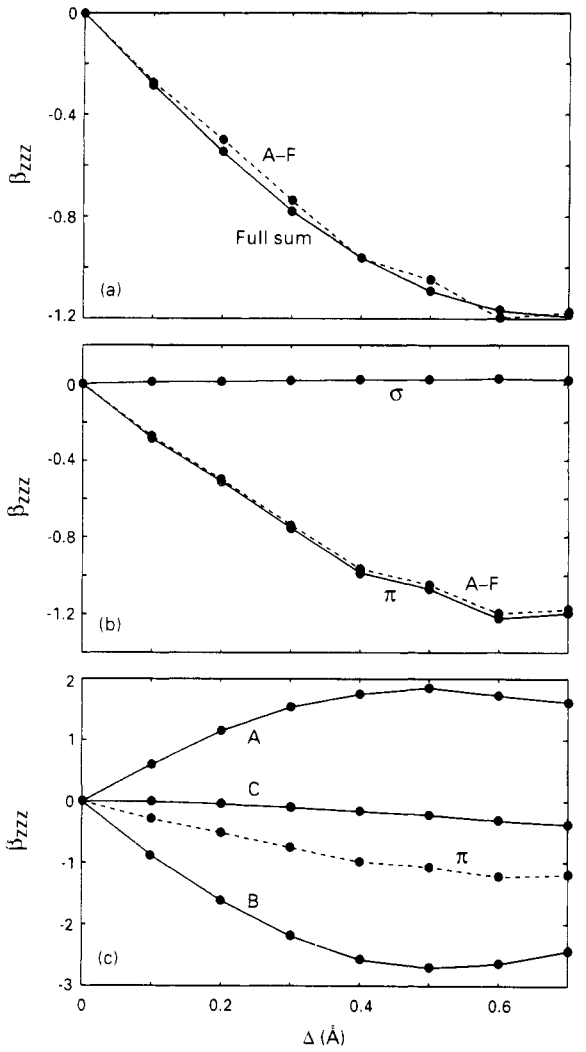

Figure 14. β_{zzz} for TiO_6^{8-} (r_0 = 1.96 Å), decomposed into π and σ contributions. (a) Values calculated using all singly-excited states (solid curve), compared with partial sum A + B + C + D + E + F (broken curve). (b) Partitioning into separate π (A + B + C) and σ (D + E + F) terms. The σ contribution is virtually nonexistent. (c) Individual π terms (A, B, C); the sum is indicated by the broken curve. Note the similarity to Figure 11a.

results indicate the importance of the diagonal A and C terms for a complete picture of the π excitations and suggest that caution must be exercised when assessing apparent differences in β at this level of theory.

Several other points are worth noting concerning the nature of the excited states involved in the largest contributions to β_{zzz}. The overwhelming majority of excited states for all values of r_0 and Δ are derived from population of the degenerate $|\pi_{xz}^*\rangle$ and $|\pi_{yz}^*\rangle$ orbitals. The sources are either the degenerate $|\pi_{xz}\rangle$ and $|\pi_{yz}\rangle$ orbitals, or one of four degenerate pairs of $|\pi_{xyz}^n\rangle$.[31] The nonbonding orbitals retain the same order in energy over the whole range of r_0 and Δ, although the mixing of atomic orbitals within a particular pair varies. All of the molecular orbitals that participate contain a π_z^n component, whereas those that do not have only π_x^n or π_y^n character. In the undistorted case, the two axial oxygen atoms contribute equally to each of the π^n orbitals. This no longer holds when Δ is nonzero, however. One pair is then largely derived from O1 (the distant oxygen), while another pair has a major contribution fron the near oxygen, O2. The remaining π^n orbitals do not show any sharp distinctions. These differences are reflected in the dependence upon Δ of the contributions to β_{zzz} from the $|\pi_{xyz}^n\rangle$ orbitals. Those contributions originating from the orbitals involving O1 fall sharply as Δ increases whereas those involving O2 grow in magnitude.

Summary

Extended Hückel/sum-over-states calculations of electronic hyperpolarizability in TiO_2 and TiO_6^{8-} are remarkably sensitive to bond lengths. Taking these two fragments as representative of those portions of the KTP crystal most relevant to its nonlinear optical properties, we have computed β for a variety of structures containing different long and short axial Ti–O bonds. State-by-state analysis reveals that (1) nonlinear optical effects arise almost entirely from excitations within the π system, (2) the net effect is the result of the small difference between two large contributions of opposite sign, and (3) β values for the TiO_2 and TiO_6^{8-} systems, despite superficial differences, are determined by very similar influences. In view of (2) it is perhaps not surprising that the SHG intensities observed from KTP isomorphs vary over very wide ranges, while the TiO_6 octahedra in the crystal structures appear to exhibit almost insignificant variations with composition.[12,13,15]

Having established these points with extended Hückel theory, in future work we intend to investigate further the properties of β by using self-consistent wave functions with excited states generated by configuration interaction. Larger systems and –Ti–O–Ti–O-chains are to be considered as well. These calculations may be expected to give some substance to the apparent correlation between the Ti–O–Ti bond angles and SHG intensities observed for many isomorphs.[12,13,15]

Registry No. KTP, 12690-20-9; Ti, 7440-32-6; O_2, 7782-44-7.

(31) Nonbonding π orbitals abound in TiO_6^{8-}. There are four triply degenerate groupings in symmetric TiO_6^{8-}, each involving different subsets of the six oxygen p functions. The form $|\pi_{xyz}^n\rangle$, for example, arises from atomic orbitals $|O1_x\rangle$, $|O1_y\rangle$, $|O2_x\rangle$, $|O2_y\rangle$, $|O3_z\rangle$, $|O4_z\rangle$, $|O5_z\rangle$, $|O6_z\rangle$, and exhibits a configuration of axial oxygen p_x orbitals similar to that in TiO_2. Other combinations involve assorted mixtures of all the oxygen p functions.